

The Role of Iron Sulfide Polymorphism in Localized H₂S Corrosion of Mild Steel

Jing Ning,^{‡,*} Yougui Zheng,^{*} Bruce Brown,^{*} David Young,^{*} and Srdjan Nešić^{*}

ABSTRACT

Localized corrosion in sour fields is a challenge persisting in the oil and gas industry, as it has frequently been seen as a cause for catastrophic failures of upstream pipelines. Hence, prediction and mitigation of H₂S localized corrosion of mild steel is of key importance for integrity management. However, the current understanding of H₂S localized corrosion mechanism(s) from numerous studies in both the laboratory and the field is far from being conclusive. In particular, the environmental conditions that may cause localized H₂S corrosion are unclear. Therefore, defining an experimental condition in the laboratory that can replicate localized corrosion in a sour environment is critical to the understanding of mechanisms of localized corrosion. The focus of the present research was to explore environmental conditions leading to localized H₂S corrosion. Severe localized corrosion was repeatedly observed in experiments when there was a simultaneous formation of greigite and/or pyrite. Based on those experimental results, a hypothesis for a mechanism of H₂S localized corrosion was proposed.

KEY WORDS: hydrogen sulfide, iron sulfide, localized corrosion, polymorphism

INTRODUCTION

Corrosion caused by the presence of H₂S and CO₂ in produced fluids is frequently encountered in pipelines during the production of oil and gas. Compared to

general CO₂ and H₂S corrosion,¹⁻⁴ localized H₂S corrosion is much less understood and less studied. This poses a key challenge for integrity management in the oil and gas industry.

In open literature, H₂S localized corrosion usually has been associated with multiple risk factors, such as the presence of elemental sulfur,⁵⁻⁹ the presence of polysulfides,¹⁰⁻¹² high salinity,¹³⁻¹⁵ flow velocity,¹⁶ a change in local water chemistry at steel surface,¹⁷ and metallurgy. In addition, corrosion and scaling mitigation strategies, such as corrosion inhibitors, alcohol and glycols, and pH stabilization, used in sour systems in the oil and gas industry, can greatly decrease the uniform corrosion, while increasing the probability for localized corrosion. Kvarekval¹⁸ have showed very strong evidence of this with examples of severe localized corrosion.

Moreover, numerous studies^{1-2,19-22} have revealed that formation of an iron sulfide layer on the steel surface usually can suppress uniform corrosion, which is related to this layer acting as a diffusion barrier and by surface blockage effect. In those studies, mackinawite was observed as the dominant iron sulfide phase. In fact, polymorphous iron sulfides have been reported as corrosion products in sour oil and gas fields²³⁻²⁵ and in laboratory experiments.^{1,26-28} A few studies²⁹⁻³¹ have been conducted to explore the impact of different iron sulfide phases on the corrosion process in sour environments. In these studies, severe localized corrosion has been reported in the presence of a mackinawite deposit layer,³⁰⁻³¹ but not in the presence of pyrrhotite and troilite.³⁰ Therefore, in the present study, the focus was on further investigation of

Submitted for publication: January 14, 2016. Revised and accepted: September 2, 2016. Preprint available online: September 2, 2016. <http://dx.doi.org/10.5006/2030>.

[‡] Corresponding author. E-mail: jn248409@ohio.edu.

^{*} Institute for Corrosion and Multiphase Technology, Ohio University, 342 West State Street, Athens, OH 45701.

localized corrosion seen in a sour environment and the possible link with iron sulfide polymorphism.

EXPERIMENTAL PROCEDURES

Experimental Methodology

A thermodynamic model³²⁻³³ (in the form of Pourbaix diagrams) was used to design experimental conditions leading to formation of different iron sulfides as corrosion products in a sour environment. The subsequent influence of a corrosion product layer containing polymorphous iron sulfides on the corrosion process of steel with focus on localized corrosion was studied. Three sets of experiments were designed and executed as described next:

Experiment #1: Experiments with spontaneous formation of polymorphous iron sulfides (mackinawite, pyrrhotite, greigite, and pyrite) were designed and conducted at 80°C, where formation of polymorphous iron sulfides would be facilitated by a relatively high temperature.

Experiment #2: Experiments with formation of greigite and pyrite triggered by changing the solution pH were designed and performed at 25°C. At these experimental conditions, only mackinawite and pyrrhotite were allowed to form for 1 week before the solution pH was changed to cause formation of greigite and/or pyrite on the basis of predictions made by Pourbaix diagrams.

Experiment #3: Experiments similar to those in set #2, except that the changes of solution pH were done after 2 d before a significant mackinawite/pyrrhotite layer formed, which is considered to be precursors to transformation into more thermodynamically stable iron sulfides such as greigite and pyrite.

Apparatus

Experiments were performed in a 2 L glass cell filled with 1 wt% sodium chloride (NaCl) electrolyte. Each experiment contained 6 to 10 square-shaped steel specimens with dimensions of 1.2 cm × 1.2 cm × 0.2 cm, hung in the glass cell using nylon string, and one cylindrical working electrode (WE) specimen with dimensions of 1.2 cm diameter × 1.5 cm length, mounted on a stationary rod, with the total volume/area ratio being 0.075 cm. The square specimens were used for surface analysis and weight loss measurements, while the stationary WE was used for electrochemical measurements. A magnetic stir bar was used to keep the solution fully mixed during the experiments. A typical three-electrode setup was used to conduct electrochemical measurements. A platinum wire was used as the counter electrode. A saturated silver-silver chloride (Ag/AgCl) electrode connected to the cell externally through a Luggin capillary was used

as the reference electrode. A mesh capped pH probe³⁴ was used to measure surface pH at a corroding surface and a glass pH probe was used to monitor bulk solution pH. A 10% volume fraction of H₂S in H₂S/N₂ mixed gas was used in this study. The concentration of H₂S was adjusted by a gas rotameter and measured by a gas sample pump using H₂S detector tubes. NaOH solution and a carbon scrubber were used to treat the gas coming out of glass cell, removing the H₂S.

Material

The test specimens were all made from API 5L X65⁽¹⁾ carbon steel. The chemical composition of this carbon steel is shown in Table 1.

Procedure

The test conditions for this series of experiments are shown in Table 2. In the beginning of each test, N₂ gas was sparged through the electrolyte to deoxygenate the solution (typically more than 4 h). An H₂S and N₂ pre-mixed gas was then sparged into the solution continuously throughout the experiment. The solution pH decreased as a result of the addition of H₂S to the solution, and was adjusted to 6.0 by using a deoxygenated 1.0 M NaOH solution. The specimens were polished to a 600 grit sandpaper finish, rinsed thoroughly with deionized water and isopropanol, ultrasonically cleaned in isopropanol, and dried by an air blower before immersion in electrolyte. Experiments were conducted following the experimental designs shown in Figures 1 through 3, which indicate the specimen removal times with specific analysis designations for each. Solution pH was adjusted to 11.5 after 7 d of exposure in Experiment #2, as indicated in Figure 2, and after 2 d of exposure in Experiment #3, as indicated in Figure 4. In both cases, the pH spontaneously decreased to pH 7.0 very quickly. While taking special care that oxygen ingress was prevented, corroded square specimens were taken out for analysis on the days indicated in the timeline, rinsed with deoxygenated DI water and deoxygenated isopropanol, blown dry using N₂, and stored in a desiccator. Scanning electron microscope (SEM) imaging was used to detect the surface morphology of the specimens; energy dispersive x-ray spectrometry (EDX) and x-ray diffraction (XRD) were applied to determine the nature of iron sulfide formed on the specimens. Alicona InfiniteFocus[†] profilometer microscope was used to analyze profilometry of specimens after the removal of corrosion product layers. The vertical

TABLE 1

Chemical Composition of 5L X65 Carbon Steel Used in Experiment (wt%)

Cr	Mo	S	V	Si	C	Fe	Ni	Mn	P
0.14	0.16	0.009	0.047	0.26	0.13	Bal.	0.36	1.16	0.009

⁽¹⁾ American Petroleum Institute (API), 1220 L Street, NW, Washington, DC 20005-4070.

[†] Trade name.

TABLE 2
Test Matrix

Description	Exp. #1	Exp. #2	Exp. #3
Temperature	80°C	25°C	25°C
Electrolyte	1 wt% NaCl brine		
Gas Composition	10% H ₂ S (volume fraction)/balance N ₂		
H ₂ S Partial Pressure	0.053 bar (5.3 kPa)	0.097 bar (9.7 kPa)	0.097 bar (9.7 kPa)
Stirring Speed	400 rpm		
Material	API 5L X65		
Initial pH	6.0		

resolution of profilometry measurements is 100 nm. Solution was drawn from the glass cell immediately before taking each steel specimen, filtered by using a 0.22 μm syringe filter to remove any iron sulfide precipitate from solution, and then measured for ferrous ion concentration using a spectrophotometric method. Bulk pH, surface pH, and open-circuit potential (OCP) were monitored throughout the experiment. Both linear polarization resistance (LPR) and weight loss (WL) methods were used to obtain corrosion rate measurements. LPR measurements were performed by polarizing the WE ± 5 mV from the OCP and scanning at 0.125 mV/s. LPR measurements were conducted every 20 min in the initial 4 h of experiments

considering instable corrosion rates initially, and then were conducted every 2 h in the rest of the experiments. The measured R_p was corrected by subtracting solution resistance, which was measured independently using electrochemical impedance spectroscopy (EIS). EIS measurements were conducted by applying an oscillating potential ± 5 mV around OCP of the WE and using the frequency range 3 mHz to 5 kHz. The theoretical B value used in calculation of LPR measurements was adjusted using weight loss results, and was found to be 13 mV/decade on average in this study.

EXPERIMENTAL RESULTS

Experiment #1: Occurrence of Localized Corrosion with Spontaneous Formation of Greigite and Pyrite

Corrosion Behavior — Figure 4 shows OCP, corrosion rate, solution pH, and ferrous ion concentration evolution monitored during the experiments. Corrosion rates obtained from LPR measurements on the WE were verified by weight loss results from the square specimens. The corrosion rate was 1.1 ± 0.3 mm/y initially and then decreased to around 0.07 ± 0.02 mm/y in the first 4 d because of the formation of a protective iron sulfide layer at steel sample surface. However, an

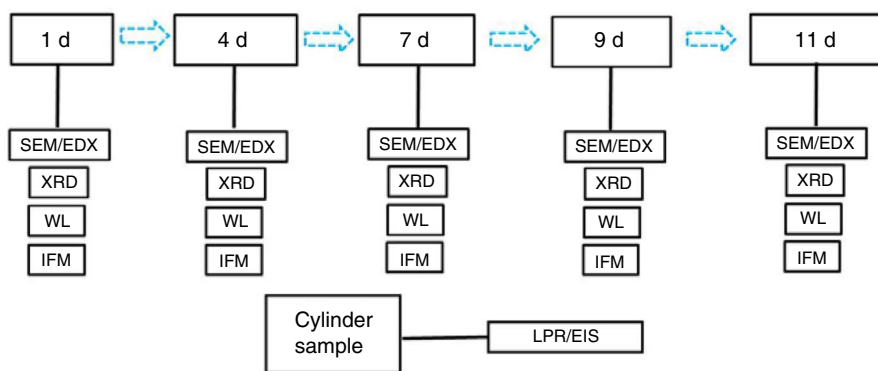


FIGURE 1. Experimental design for Experiment #1.

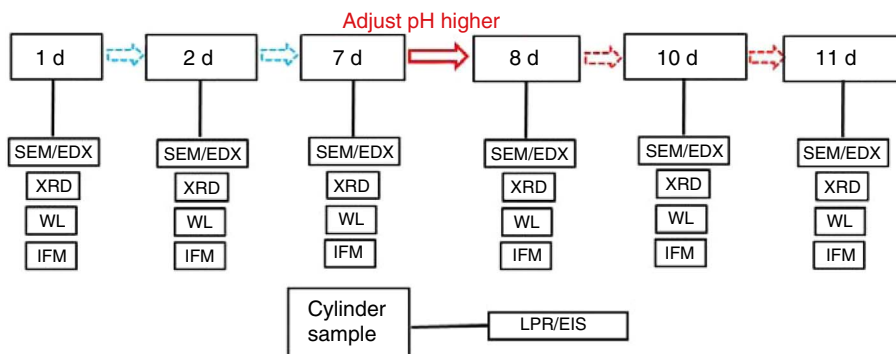


FIGURE 2. Experimental design for Experiment #2.

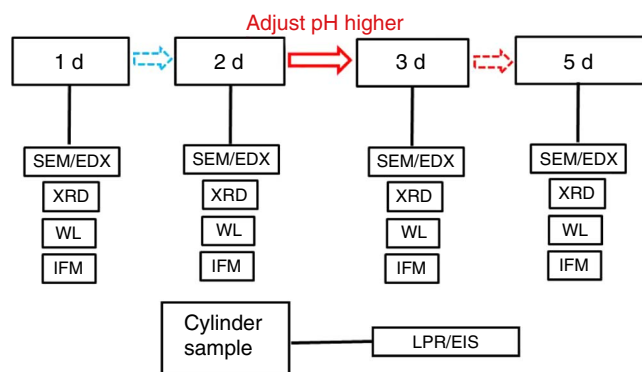


FIGURE 3. Experimental design for Experiment #3.

increase in both OCP and corrosion rate (with the exception of the high initial values) was observed after 4 d of exposure, which could be explained by an increase in cathodic reaction rate, but the cause of this was yet unknown. It was hypothesized that this increase in cathodic reaction rate was a result of either the collapse of the protective corrosion product layer increasing transport of corrosive species required for cathodic reactions or the formation of conductive corrosion products increasing the overall cathodic reaction area.

Corrosion Products — Figure 5 presents surface morphologies of the square specimens as removed in chronological order. A uniform surface morphology was observed after 1 d and 4 d of exposure, while blistering, cracking, and spalling morphologies were seen after 7 d, 9 d, and 11 d of the experiment.

Table 3 summarizes the XRD quantitative analysis of corrosion products determined by the reference intensity ratio (RIR) methodology in order to better understand formation and transformation of polymorphous iron sulfide phases throughout the experiment. This table clearly shows a transformation of the initial thermodynamically metastable mackinawite to the more stable pyrrhotite and pyrite phases. Mackinawite accounts for 90% of corrosion products formed after 1 d of exposure, while decreasing significantly

over exposure duration. In contrast, both pyrrhotite and pyrite phases have a dramatic increase throughout the experiment. In addition, the formation of greigite was indicated as a corrosion product after 1 d through 9 d of exposure, but was not observed on the last sample from the experiment. That is because greigite is also a metastable phase, developed from the initial mackinawite and then transformed completely to the final thermodynamically stable pyrite after 11 d.

To have a closer look at the corrosion product layer, surface morphology and cross-section SEM images of samples after 4 d and after 7 d, at a higher magnification, are shown in Figure 6. A lot of small cubic crystals were observed on the mackinawite layer in the surface SEM images of samples shown in Figures 6(a) and (b), which are believed to be pyrite crystals on the basis of XRD findings. Further, cross-section images presented in Figures 6(c) and (d) are backscattered electron composition (BEC) images, which show atomic differences by changes of contrast in the image. In general, darker areas that appear in BEC images are atomically lighter, while brighter areas are atomically heavier. Accordingly, the crystals with lighter color on top of the gray mackinawite layer are considered to be pyrite, as seen on the surface SEM images in Figures 6(a) and (b). Note that there are many crystals with the lighter color embedded in the darker mackinawite layers of the cross-section sample, suggesting that pyrite crystals are also embedded in the mackinawite layer. Furthermore, a steady increase in the thickness of the iron sulfide layer formed on steel surface throughout experiment was observed. Hence, the first hypothesis that was proposed for the increase in both OCP and corrosion rate when there was initiation of localized corrosion, stating that a loss of diffusion barrier layer would increase the transport of corrosive species, is proven to be wrong. Therefore, the second hypothesis, the formation of a conductive corrosion product layer (an iron sulfide layer containing pyrite in this study) increasing overall cathodic reaction area, was taken into consideration.

Surface Profilometry of Samples after Removing Corrosion Product Layer — The corrosion product layer

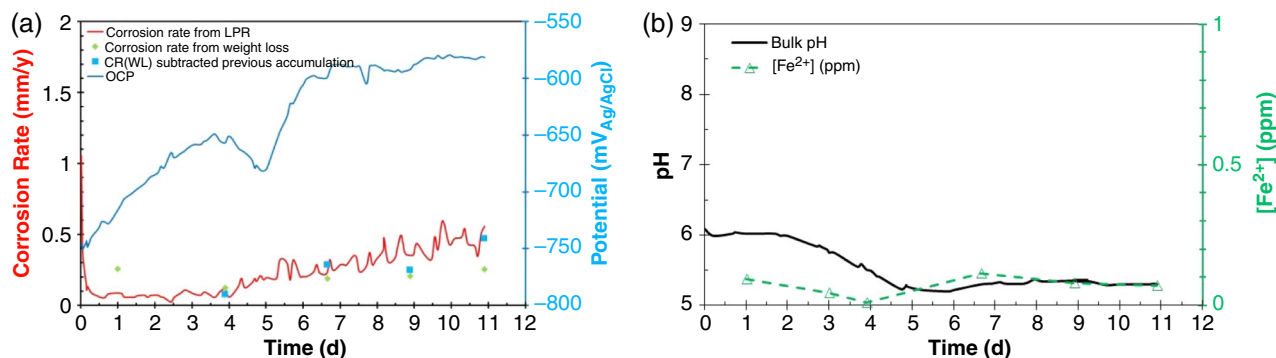


FIGURE 4. Parameters monitored throughout Experiment #1: (a) OCP and corrosion rate, and (b) bulk pH and [Fe²⁺].

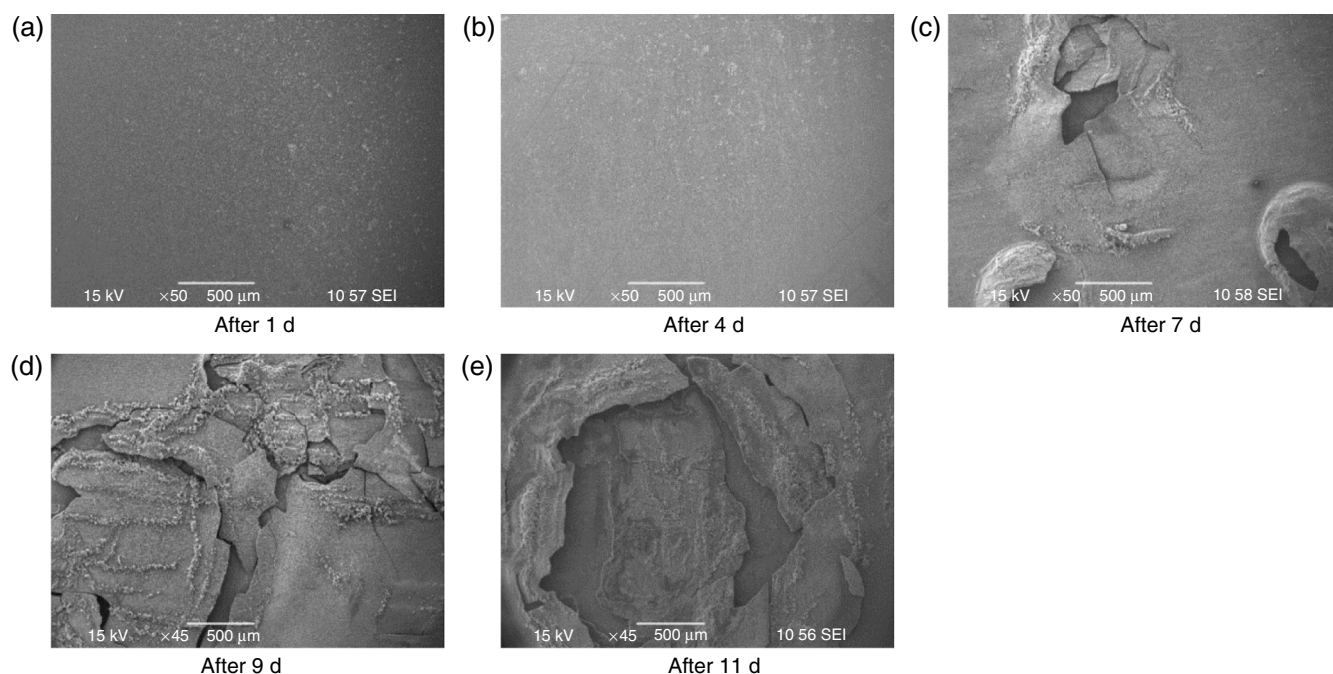


FIGURE 5. Surface morphologies of samples: (a) after 1 d, (b) after 4 d, (c) after 7 d, (d) after 9 d, and (e) after 11 d.

TABLE 3

XRD Quantitative Analysis of Corrosion Products Formed in Experiment #1

Phases	Chemical Formula	1 d (%)	4 d (%)	7 d (%)	9 d (%)	11 d (%)
Mackinawite	FeS	90.0	76.4	49.2	63.6	66.0
Pyrrhotite	FeS	8.0	5.8	14.8	1.9	16.4
Greigite	Fe ₃ S ₄	2.0	2.2	3.3	3.3	0
Pyrite	FeS ₂	0	4.8	27.8	18.5	10.6
Iron Carbide	Fe ₃ C	0	10.8	4.9	12.7	7.0

was removed by using Clarke's solution³⁵ and a cleaning method as outlined in ASTM G1³⁶ to observe the corroded steel underneath. A flat surface owing to uniform corrosion after 4 d of the test was seen in Figure 7(a). Then, initiation of localized corrosion was observed as 10 μm deep pits after 7 d in Figure 7(b). And finally, propagation of localized corrosion can be observed in Figures 7(c) and (d). At the end of this experiment, after 11 d of exposure, a 40 μm depth of localized corrosion was measured. The penetration rate based on this 40 μm depth was calculated to be 2.1 mm/y. As compared to the general corrosion rate in the initial 4 d of 0.07 mm/y, significant localized corrosion occurred. It should be noted that the localized corrosion occurred when quantitative analysis shows higher concentrations of greigite and/or pyrite in the corrosion product, which indicates a possible correlation between localized corrosion and the formation of greigite and/or

pyrite. This correlation between spontaneous formation of pyrite and the occurrence of localized corrosion was later confirmed in other similar corrosion experiments conducted at high temperature,³⁷ which are a subject of a separate publication being currently prepared. This hypothesis was further verified in the following experiments.

Experiment #2: Localized Corrosion Triggered by Formation of Greigite/Pyrite

Experiment #1 indicated a possible correlation between localized corrosion and the spontaneous formation of greigite and/or pyrite at high temperature (80°C). However, a correlation does not indicate causation, i.e., it was not certain whether the spontaneous formation of greigite and/or pyrite was a cause of localized corrosion or if it happened approximately at the same time for some yet unknown reason, or possibly even as a consequence of localized corrosion. To distinguish these possibilities, experiments were organized at conditions where greigite and/or pyrite do not form readily (at 25°C) and where their formation can be induced at will by (for example) changing the pH. The assumption was that this would lead to localized corrosion. Therefore, in Experiment #2 conditions were set such that only mackinawite and pyrrhotite formed initially, and then the solution pH was increased after 7 d of exposure to trigger greigite and/or pyrite formation, all this according to Pourbaix diagrams. To illustrate this approach, Figure 8 shows Pourbaix diagrams generated at the experimental

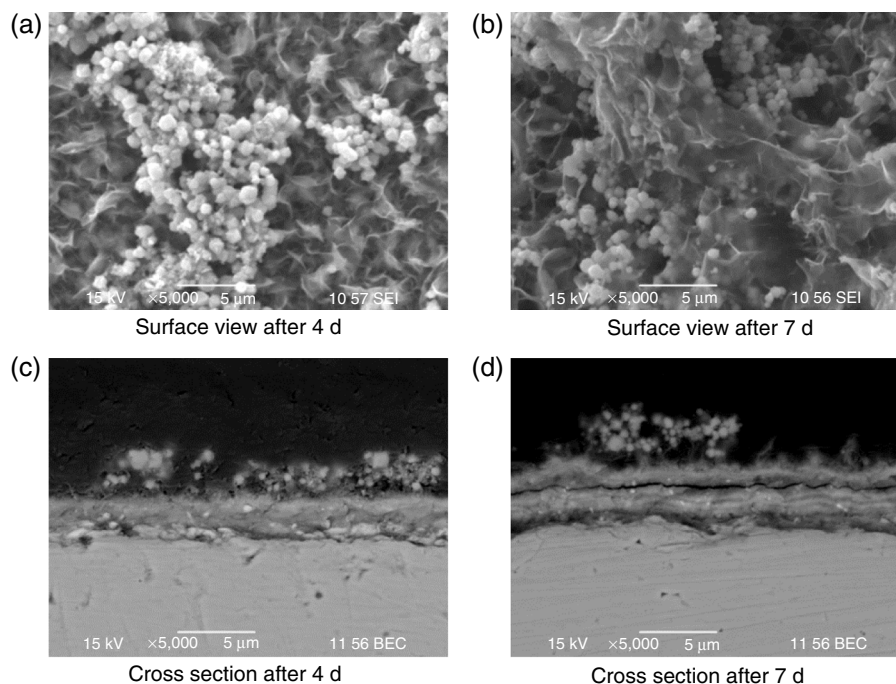


FIGURE 6. SEM images with 5,000 \times magnification: (a) surface view after 4 d, (b) surface view after 7 d, (c) cross section after 4 d, and (d) cross section after 7 d.

conditions after 7 d of exposure, and, accordingly, greigite and/or pyrite are expected to form if the solution pH is adjusted from a low original value (around pH 5) to a high value (above pH 11).

Corrosion Behavior—Figure 9(a) shows bulk pH and surface pH monitored during this experiment. As mentioned, solution pH was adjusted from pH 5.5 to 11.5 after 7 d of exposure using deoxygenated NaOH solution, but quickly decreased spontaneously to approximately pH 7.0. Figure 9(b) shows the OCP and corrosion rates throughout the experiment. Both corrosion rates and OCP were very stable throughout the initial 7 d of experiment, but did have a significant increase immediately after adjusting the solution pH and kept slowly increasing until the end of the experiment. In addition, weight loss was also performed, confirming LPR measurements. It is noteworthy that weight loss results were corrected by subtracting from previous accumulation in order to properly compare them with LPR measurements. As shown in Figure 9, this experiment was repeated twice with almost identical results.

Corrosion Products—Table 4 shows the quantitative analysis of corrosion products formed on samples during this experiment. The formation of greigite after adjustment of solution pH is obvious, as the percentage of the greigite phase changes from zero before pH adjustment to 9.0% after the pH adjustment and to 17.9% after the 11th day of the experiment. Pyrite was also observed on the last sample. In addition, a

decrease in the mackinawite phase can be observed from 90.8% after 7 d to 78.6% after 11 d.

Figure 10 presents the comparison of surface morphologies of samples from Experiment #2. A uniform corrosion product layer was observed on samples in advance of the pH adjustment, as shown in Figures 10(a) through (c). However, spalling and exfoliation of a corrosion product layer can be seen on samples after the adjustment of solution pH, shown in Figures 10(d) through (f).

Surface Profilometry of Samples After Removing Corrosion Product Layer—Figure 11 shows surface profilometry of samples after removing the iron sulfide layer. The sample before pH adjustment shown in Figure 11(a) presents a flat surface resulting from a 0.3 mm/y general corrosion rate; in contrast, the sample after adjusting pH in Figure 11(b) shows a locally corroded surface with a 14.6 mm/y pit penetration rate (assuming this localized corrosion occurred in 1 d). Again, significant localized corrosion was clearly observed when there was a high content of greigite and/or pyrite phases. In addition, an increase in both OCP and corrosion rate was observed again when localized corrosion occurred. This experiment was repeated and the experimental results were reproducible. After the pH adjustment, a dramatic increase in both OCP and corrosion rate was observed, both greigite and pyrite as new corrosion product phases were detected, and severe localized corrosion occurred with approximately the same penetration rate.

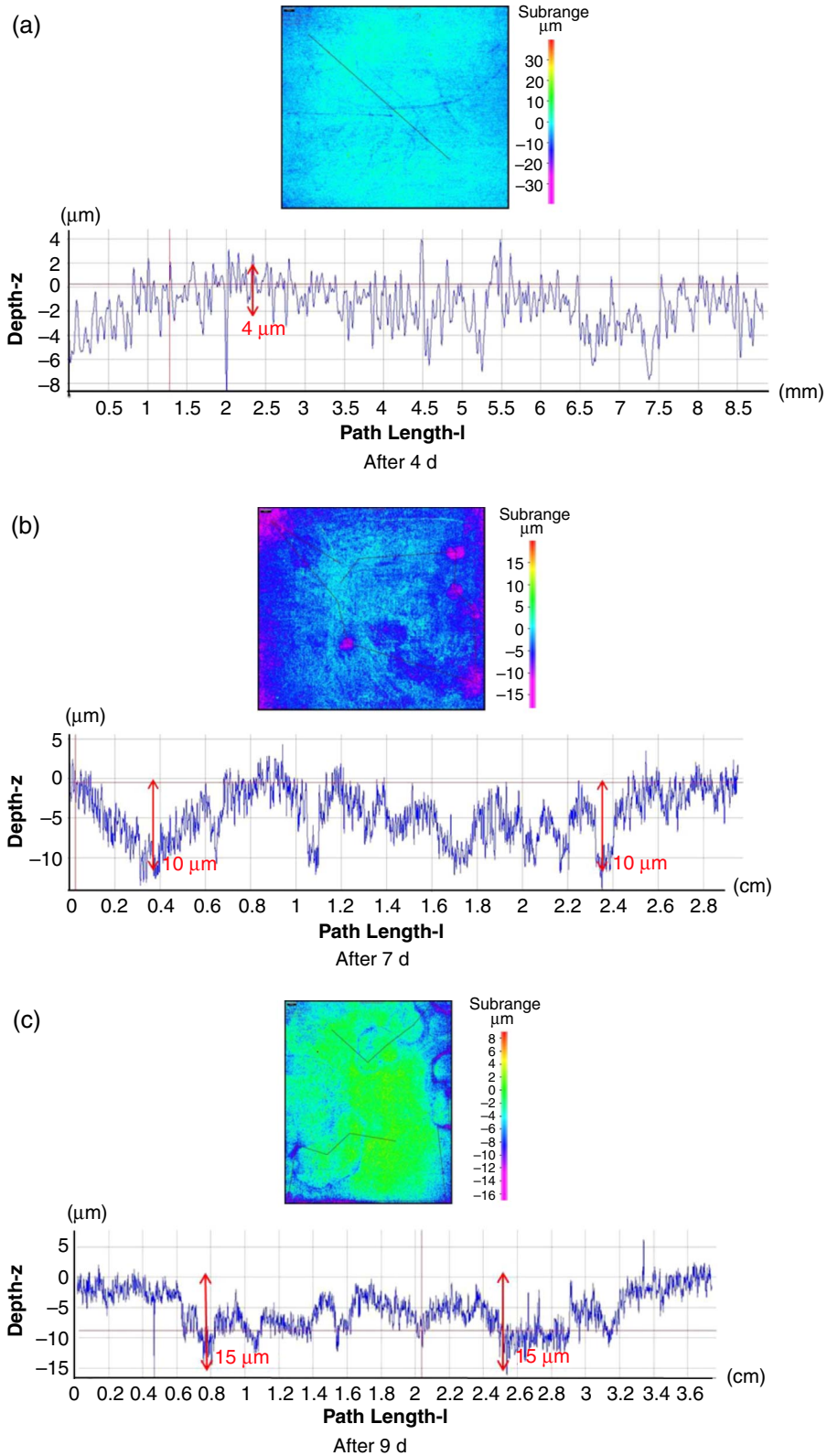


FIGURE 7. Surface profilometry of samples after removing corrosion product layer: (a) after 4 d, (b) after 7 d, (c) after 9 d, and (d) after 11 d.

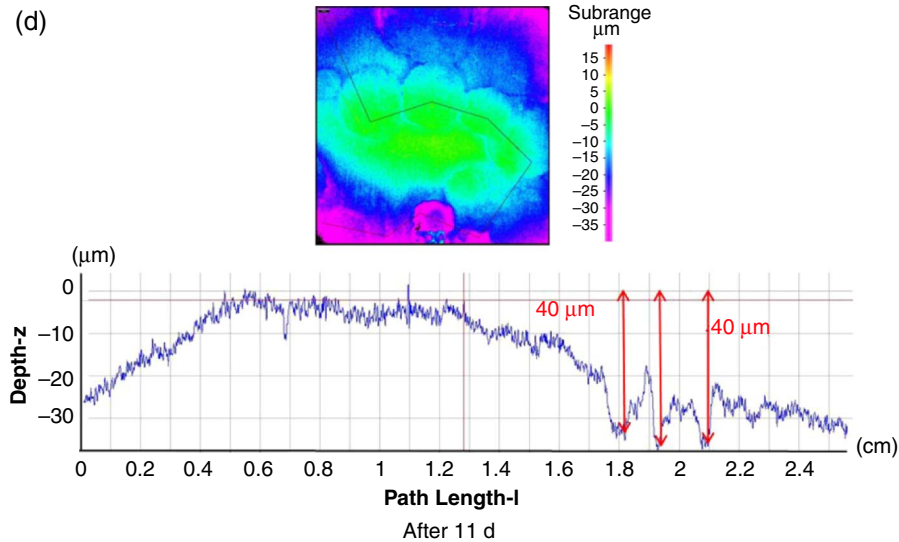


FIGURE 7. (Continued).

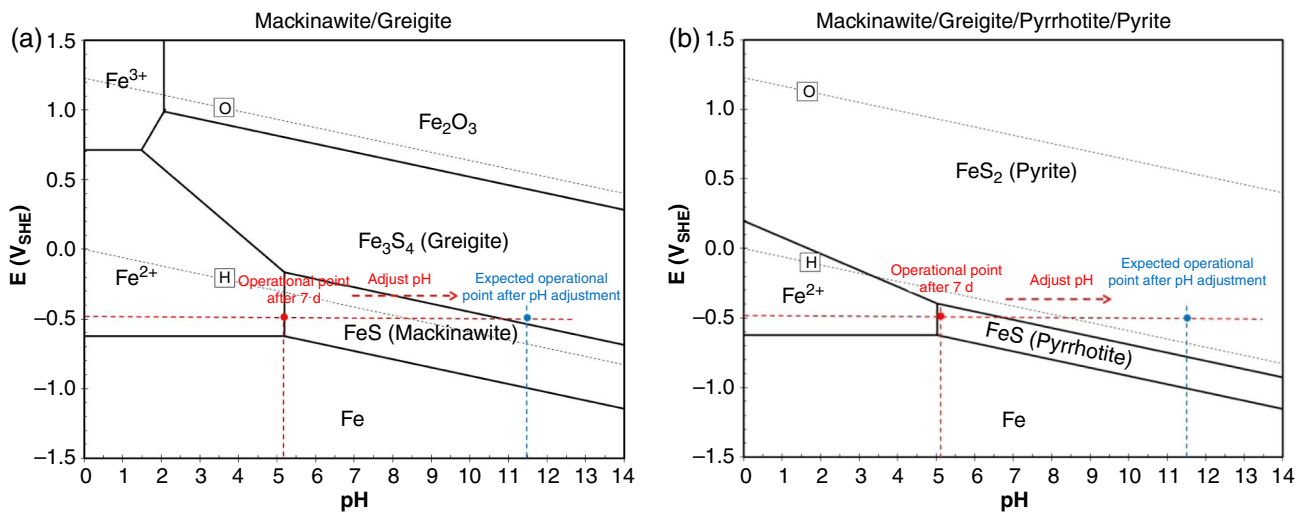


FIGURE 8. Thermodynamic considerations for the formation of iron sulfides triggered by adjusting pH at 25°C according to Pourbaix diagram predictions (Pourbaix diagram was generated at $T = 25^\circ\text{C}$, $p\text{H}_2\text{S} = 9.7 \text{ kPa}$ [0.097 bar], $[\text{Fe}^{2+}] = 0.52 \text{ ppm}$, $[\text{Fe}^{3+}] = 1.0 \times 10^{-6} \text{ M}$): (a) only mackinawite/greigite considered and (b) all expected iron sulfides considered.

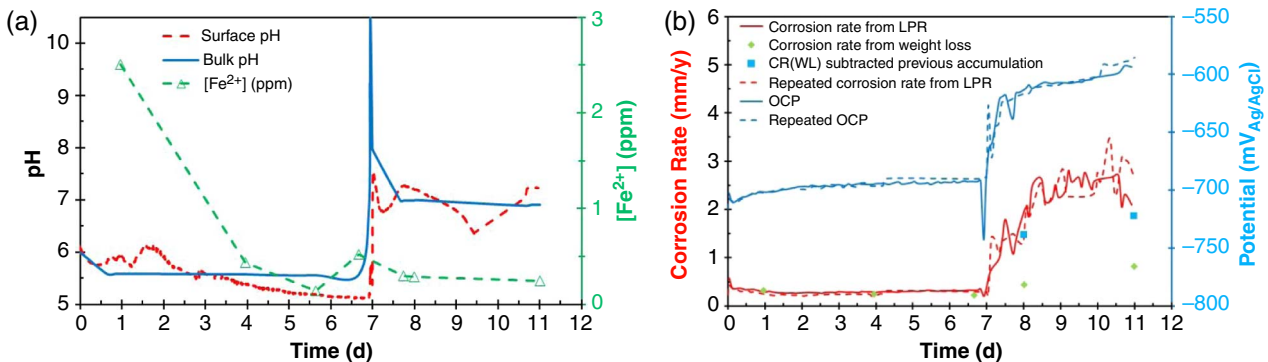


FIGURE 9. Parameters monitored throughout Experiment #2: (a) bulk pH, surface pH, and $[\text{Fe}^{2+}]$, and (b) corrosion rates and OCP.

TABLE 4

XRD Quantitative Analysis of Corrosion Products Formed in Experiment #2 (1st repeat)

Phases	Chemical Formula	7 d (%)	8 d (%)	11 d (%)
Mackinawite	FeS	90.8	90.4	78.6
Pyrrhotite	FeS	5.2	0.3	0
Greigite	Fe ₃ S ₄	0	9.0	17.9
Pyrite	FeS ₂	0	0	3.2
Iron Carbide	Fe ₃ C	4.0	0.3	0.3

Experiment #3: Adjusting Solution pH Prior to Formation of Greigite/Pyrite

Experiment #2 provided strong evidence that there is a correlation between the localized corrosion and the formation of greigite and/or pyrite triggered by adjusting solution pH after 7 d of exposure. However, it was also possible that the localized corrosion occurred in Experiment #2 was not related to the formation of greigite and/or pyrite but was a result of the formation of elemental sulfur and/or polysulfides at high pH condition.⁹⁻¹² Therefore, one more experimental condition was designed and executed to better understand the mechanism for this type of localized corrosion in sour environments and confirm that it was indeed a result of formation of greigite and/or pyrite. In the present experiment, the solution pH was adjusted after 2 d rather than 7 d as done in the previous experiment. The idea was that this was insufficient time for the development of a full mackinawite layer, which is a precursor for the transformation into more

thermodynamically stable greigite and pyrite. In this experiment, the formation of greigite and/or pyrite after the pH adjustment and the occurrence of localized corrosion were not expected.

Corrosion Behavior — Figure 12 shows pH values monitored during this experiment. The pH behavior of the present experiment was reproduced exactly the same as in Experiment #2, but with the exception that solution pH was adjusted after 2 d of exposure.

Figure 13 shows OCP and corrosion rates monitored during the present experiment. A marked increase in the OCP after adjusting pH was observed, which is similar to Experiment #2. However, the corrosion rate was stable throughout the experiment, which is different from Experiment #2, where there was an increased corrosion rate immediately after the pH adjustment.

Corrosion Products — Figure 14 shows surface morphologies of the specimen surface. Before the pH adjustment (after 1 d and after 2 d of the test), a partially covered surface with corrosion product layer was observed on those samples. After the pH adjustment was performed, a uniform and fully covered corrosion product layer with lots of clusters on top of the layer was seen on the samples after 3 d and after 5 d of test, which is believed to be mackinawite precipitated at high pH conditions.

Table 5 presents XRD findings of corrosion products formed on those samples. For the samples before the pH adjustment, only mackinawite was detected. After the pH adjustment, a mixture of dominant mackinawite and pyrrhotite was observed. Neither greigite nor pyrite was detected after the pH adjustment. This is

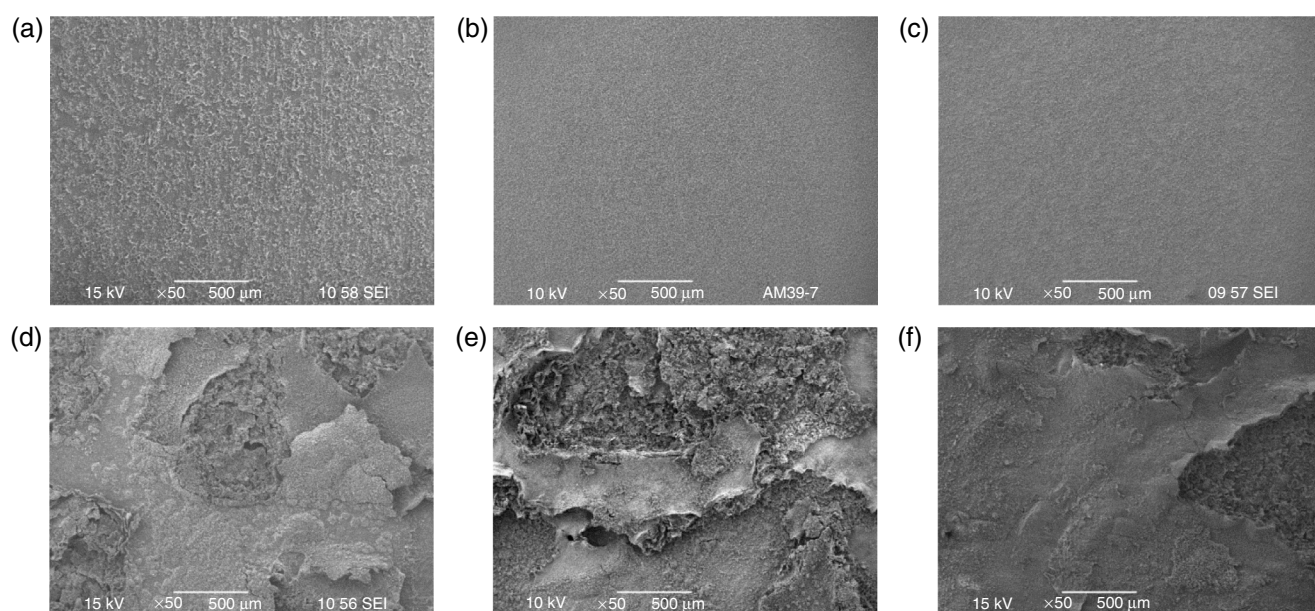


FIGURE 10. Surface morphologies of samples from Experiment #2 (1st repeat) in chronological order: (a) after 1 d, (b) after 4 d, (c) after 7 d, (d) after 8 d, (e) after 10 d, and (f) after 11 d.

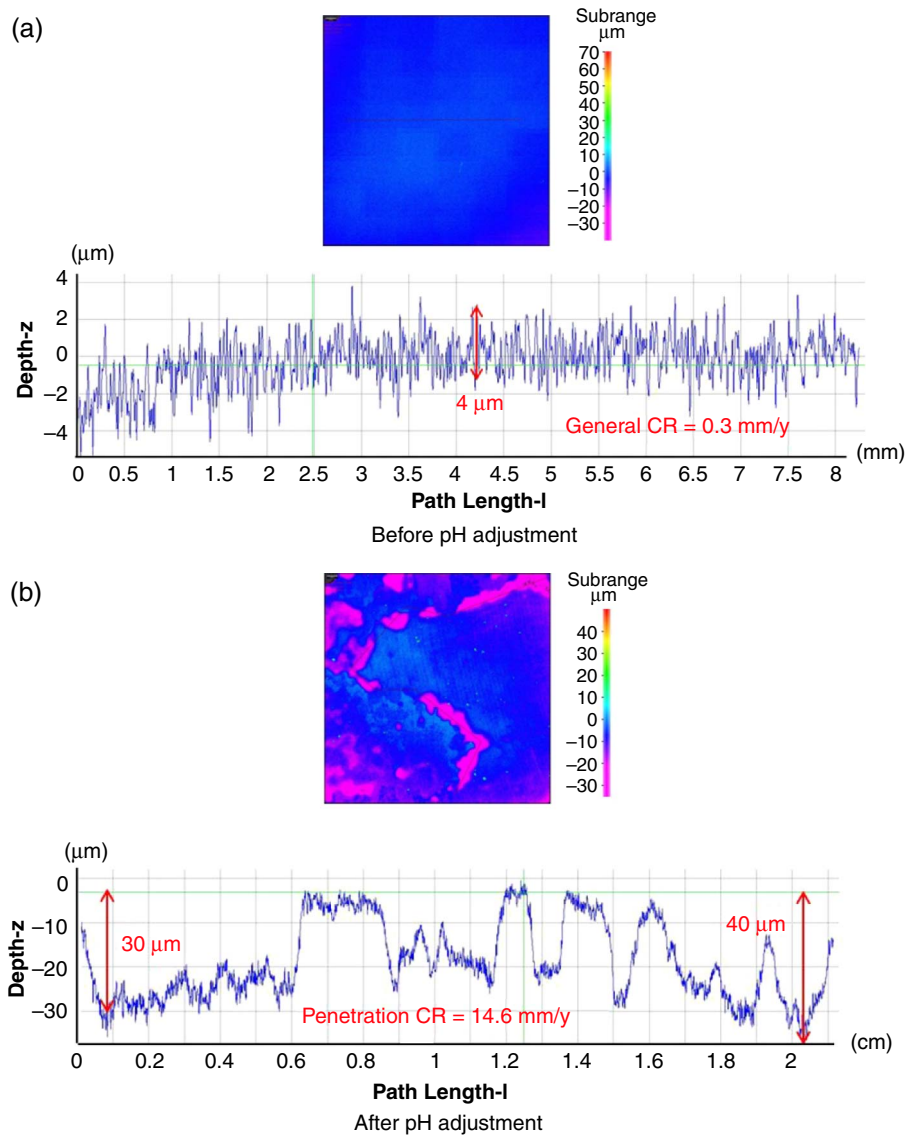


FIGURE 11. Surface profilometry of samples from Experiment #2 (1st repeat) after removing corrosion product layer: (a) after 7 d and (b) after 8 d.

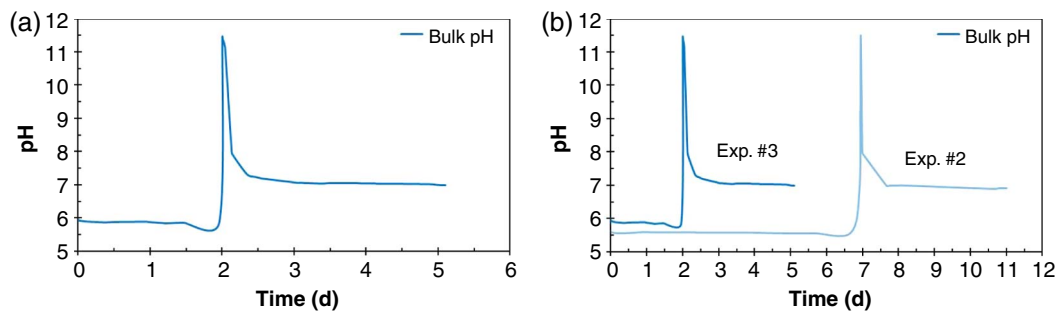


FIGURE 12. (a) pH values monitored during Experiment #3 and (b) comparison of pH values between Experiments #2 and #3.

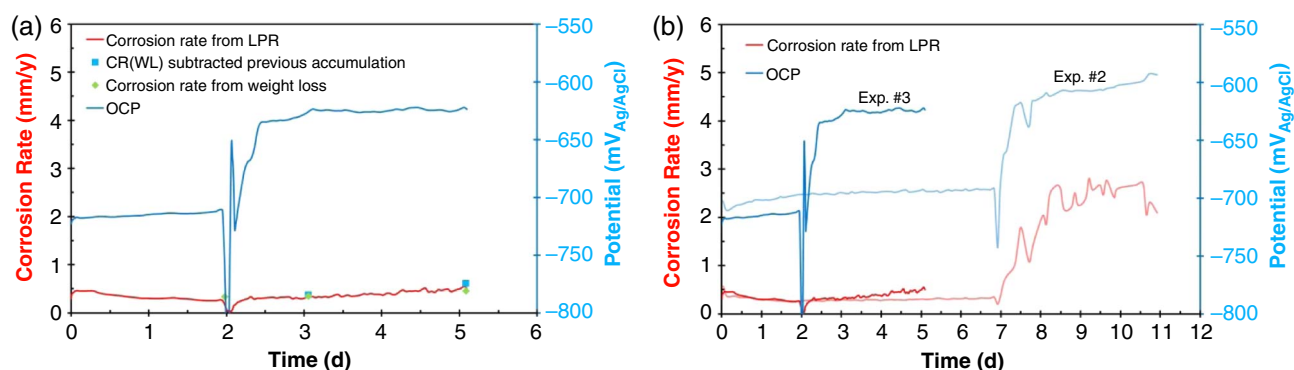


FIGURE 13. (a) OCP and corrosion rate throughout Experiment #3, and (b) comparisons of corrosion rate and OCP between Experiments #2 and #3.

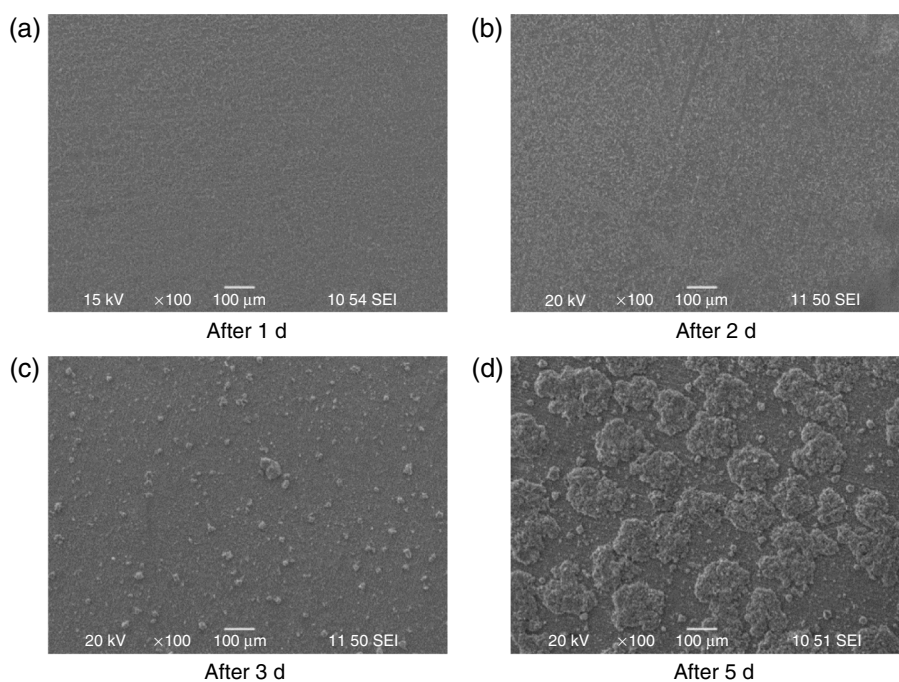


FIGURE 14. Surface morphologies of samples: (a) after 1 d, (b) after 2 d, (c) after 3 d, and (d) after 5 d.

TABLE 5

XRD Quantitative Analysis of Corrosion Products Formed in Experiment #3

Phases	Chemical Formula	2 d (%)	3 d (%)	5 d (%)
Mackinawite	FeS	100	93.8	89.1
Pyrrhotite	FeS	0	2.1	7.3
Greigite	Fe ₃ S ₄	0	0	0
Pyrite	FeS ₂	0	0	0
Iron Carbide	Fe ₃ C	0	4.1	3.6

probably attributed to an insufficient time for the development of sufficient mackinawite, which is considered to be a precursor for transformation into greigite and pyrite.

Surface Profilometry of Samples After Removing Corrosion Product Layer — The corrosion product layer was removed to check if localized corrosion occurred in the present experiment, particularly after the pH adjustment. A relatively flat surface indicating uniform corrosion before the pH adjustment was seen in Figure 15(a). After the pH adjustment, a flat surface was observed on the sample after 3 d of exposure in Figure 15(b), and also on the sample after 5 d of test in Figure 15(c). Based upon the profilometry of these samples before and after pH adjustment, localized corrosion did not occur in the present experiment. This result confirms the fact that the localized corrosion observed in Experiment #2 was not a result of elemental sulfur and/or polysulfide formation in the solution at

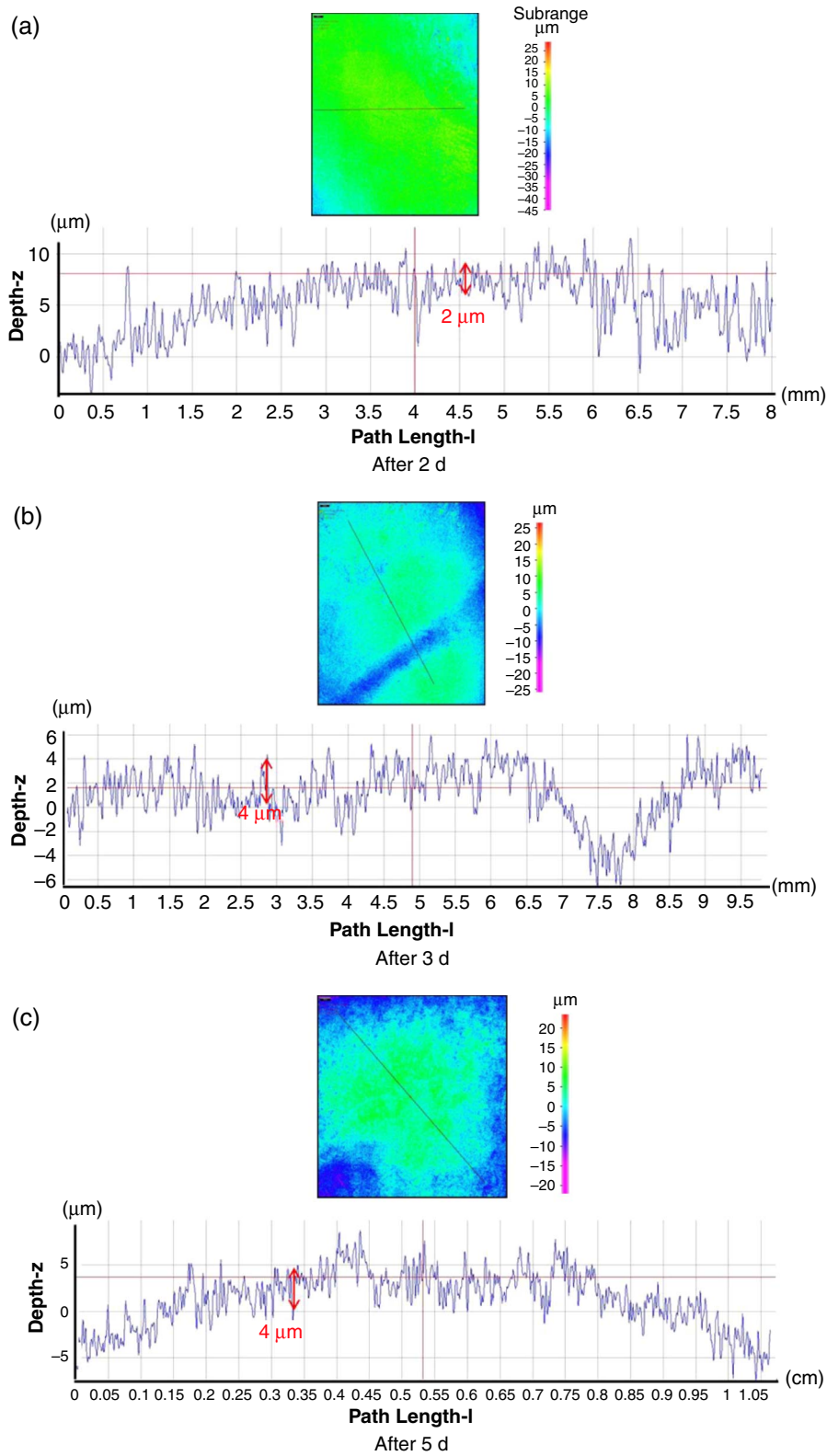


FIGURE 15. Surface profilometry of samples: (a) after 2 d, (b) after 3 d, and (c) after 5 d.

the high pH conditions. Although high pH conditions were reproduced, it seems that the development of mackinawite was insufficient for transformation into greigite and/or pyrite. Given that neither greigite nor pyrite was detected after the pH adjustment, this is proof of a strong connection between localized corrosion and the formation of greigite and/or pyrite.

SUMMARY

Based on these three sets of experiments, localized corrosion was observed only in conditions where there was formation of sufficient amount of greigite and/or pyrite (including both spontaneous formation at high temperature and formation at low temperature, triggered by adjusting solution pH). Localized corrosion was not found when greigite and pyrite did not form. All of these experiments indicate that there is a strong correlation between the localized corrosion and the formation of greigite and/or pyrite. That is, formation of greigite and/or pyrite probably plays an important role in the initiation of localized corrosion. However, the mechanism of this type of localized corrosion related to the formation of greigite and/or pyrite is not yet clear. It may be a result of a galvanic effect exaggerated by the difference in electrical conductivity associated with polymorphous iron sulfides³⁸⁻⁴² or it may be a result of the local acidification at the steel sample surface¹⁷ during the transformation process to greigite and/or pyrite. This is a topic of further study.

CONCLUSIONS

- ❖ In the current experimental conditions, severe localized corrosion was observed in experiments when there was formation of greigite and/or pyrite. Localized corrosion was not found when neither greigite nor pyrite formed.
- ❖ The formation of greigite and/or pyrite plays an important role in the initiation of the localized corrosion.
- ❖ A further comprehensive study is required to investigate this correlation between localized corrosion and greigite and/or pyrite formation.

ACKNOWLEDGMENTS

The authors would like to express sincere appreciation to the following industrial sponsors for their financial support and direction: Anadarko, Baker Hughes, BP, Chevron, Clariant Oil Services, CNPC Tubular Goods, ConocoPhillips, DNV GL, Hess, INPEX Corporation, M-I SWACO, Multi-Chem, Nalco Champion, Occidental Oil Company, Petrobras, Petroleum Development Oman, Petroleum Institute (GRC), Petronas, PTT, Saudi Aramco, Sinopec, TransCanada, TOTAL, and Wood Group Integrity Management. The authors also appreciate the help offered at the Center for

Electrochemical Engineering Research, Department of Chemical and Biomolecular Engineering at Ohio University, enabling the use of the XRD.

REFERENCES

1. W. Sun, "Kinetics of Iron Carbonate and Iron Sulfide Scale Formation in CO₂/H₂S Corrosion" (Ph.D. diss., Ohio University, 2006).
2. B. Brown, "The Influence of Sulfides on Localized Corrosion of Mild Steel" (Ph.D. diss., Ohio University, 2013).
3. Y. Zheng, "Electrochemical Mechanism and Model of H₂S Corrosion of Carbon Steel" (Ph.D. diss., Ohio University, 2015).
4. Y. Zheng, J. Ning, B. Brown, S. Nešić, *Corrosion* 71, 3 (2015): p. 316-325.
5. D.W. Davis, R.A. Detro, "Fire and Brimstone The History of Melting Louisiana's Sulphur," Louisiana Geological Survey, 1992.
6. D.D. MacDonald, B. Roberts, J.B. Hyne, *Corros. Sci.* 18, 5 (1978): p. 411-425.
7. N.I. Dowling, P.D. Clark, J.B. Hyne, *Alberta Sulphur Research Center Quarterly Bulletin XXXIII*, 1 (1996): p. 15-28.
8. N.I. Dowling, "Corrosion of Materials Used in Storage and Handling of Solid Elemental Sulphur," Proc. of the International Symposium on Materials Performance: Sulphur and Energy, 31st Annual Conference of Metallurgists of CIM (Edmonton, Canada: CIM, 1992), p. 103-115.
9. H. Fang, "Investigation of Localized Corrosion of Carbon Steel in H₂S Environments" (Ph.D. diss., Ohio University, 2011).
10. G. Schmitt, *Corrosion* 47, 4 (1991): p. 285-308.
11. H.U. Schutt, P.R. Rhodes, *Corrosion* 52, 12 (1996): p. 947-952.
12. A. Kamyshny Jr., A. Gofman, J. Gun, D. Rizkov, O. Lev, *Environ. Sci. Technol.* 38 (2004): p. 6633-6644.
13. T.W. Hamby, *J. Petrol. Technol.* (1981): p. 792-798.
14. H. Fang, B. Brown, S. Nešić, *Corrosion* 69, 3 (2013): p. 397-302.
15. H. Fang, B. Brown, S. Nešić, *Corrosion* 67, 1 (2011): p. 015001-1 to 015001-12.
16. S. Nešić, "Carbon Dioxide Corrosion of Mild Steel," in *Uhlig's Corrosion Handbook*, ed. R.W. Revie, 3rd ed. (Hoboken, NJ: John Wiley & Sons Inc., 2011), p. 229-245.
17. J. Vera, "Passivity of Iron and its Breakdown in Alkaline Sulfide Solutions" (Ph.D. diss., Rice University, 1984).
18. J. Kvarekval, "Morphology of Localized Corrosion Attacks in Sour Environments," CORROSION 2007, paper no. 659 (Houston, TX: NACE International, 2007).
19. W. Sun, S. Nešić, S. Papavinasam, *Corrosion* 64, 7 (2008): p. 586-599.
20. E. Abelev, J. Sellberg, T.A. Ramanarayanan, S.L. Bernasek, *J. Mater. Sci.* 44 (2009): p. 6167-6181.
21. Y. Zheng, J. Ning, B. Brown, D. Young, S. Nešić, *Corrosion* 72, 5 (2016): p. 679-691.
22. Y. Zheng, B. Brown, S. Nešić, *Corrosion* 70, 4 (2014): p. 351-365.
23. T.A. Ramanarayanan, S.N. Smith, *Corrosion* 46, 1 (1990): p. 66-74.
24. B. Craig, *MP* 8 (2002): p. 56-58.
25. S.N. Smith, *MP* 8 (2013): p. 44-47.
26. K. Lee, "A Mechanistic Modeling of CO₂ Corrosion of Mild Steel in the Presence of H₂S" (Ph.D. diss., Ohio University, 2004).
27. M. Singer, A. Camacho, B. Brown, S. Nešić, *Corrosion* 67, 8 (2011): p. 085003-1 to 085003-16.
28. M. Singer, J.N. Al-Khamis, S. Nešić, *Corrosion* 69, 6 (2013): p. 624-638.
29. S.M. Wilhelm, "Galvanic Corrosion Caused by Corrosion Products," in *Galvanic Corrosion*, ed. H.P. Hack, ASTM STP 978 (Philadelphia, PA: ASTM International, 1988), p. 23.
30. C.M. Menendez, V. Jovancevic, S. Ramachandran, M. Morton, D. Stegmann, *Corrosion* 69, 2 (2013): p. 145-156.
31. R.L. Martin, R.R. Annand, *Corrosion* 37, 5 (1981): p. 297-301.
32. J. Ning, Y. Zheng, D. Young, B. Brown, S. Nešić, *Corrosion* 70, 4 (2014): p. 375-389.
33. J. Ning, Y. Zheng, D. Young, B. Brown, S. Nešić, *Corrosion* 71, 8 (2015): p. 945-960.
34. J. Han, B. Brown, D. Young, S. Nešić, *J. Appl. Electrochem.* 40 (2010): p. 683-690.
35. S.G. Clarke, *Trans. Electrochem. Soc.* 69, 1 (1936): p. 131-144.
36. ASTM G1-03, "Standard Practice for Preparing, Cleaning, and Evaluating Corrosion Test Specimens" (West Conshohocken, PA: ASTM International, 2011).

37. S. Gao, "Formation of Iron Sulfide and Iron Oxide at High Temperature and Their Effects on Corrosion," Advisory Board Meeting, Ohio University, March 2016.
38. A.J. Devey, "Computer Modeling Studies of Mackinawite, Greigite and Cubic FeS" (Ph.D. diss., University College London, 2009).
39. C. Pearce, R. Patrick, D. Vaughan, *Rev. Mineral. Geochem.* 61 (2006): p. 127-180.
40. R. Schieck, A. Hartmann, S. Fiechter, R. Konenkamp, H. Wetzel, *J. Mater. Res.* 5, 7 (1990): p. 1567-1572.
41. M. Caban-Acevedo, M.S. Faber, Y. Tan, R.J. Hamers, S. Jin, *Nano Lett.* 12, 4 (2012): p. 1977-1982.
42. P.K. Abraitis, R.A.D. Patrick, D.J. Vaughan, *Int. J. Miner Process* 74 (2004): p. 41-59.